Journal of Thermal Analysis and Calorimetry (2022) 147:8791–8802
https://doi.org/10.1007/s10973-021-11170-x

Mitigation of NO_x and CO_2 from diesel engine with EGR and carbon capture unit

Pulkit Kumar[1] · Ajit Kumar Parwani[1] · Mohammad Mehdi Rashidi[2,3]

Received: 19 May 2021 / Accepted: 28 November 2021 / Published online: 22 January 2022

Abstract

The significant contribution of NO_x and CO_2 emissions with Diesel engines and stringent European Standard norms have compelled many researchers to seek new technologies for an effective solution. Exhaust gas recirculation (EGR) can control NO_x emission but at the cost of increasing CO_2 emission. This trade-off is addressed in this research work where the theoretical design of a Diesel engine retrofitted with devices for simultaneous mitigation of NO_x and CO_2 has been presented. The simulation of the combustion process of the Diesel engine has been performed by the commercial software ANSYS which indicates 32.9%, 50.63%, and 54.43% reduction of NO_2 with 10%, 20%, and 30% EGR ratio, respectively, while the corresponding increase of CO_2 is 4.76%, 9.52%, and 15.28%, respectively. The mitigation of this increased amount of CO_2 has been demonstrated by carrying out experimental investigations on Diesel engine exhaust with carbon capture unit using two standalone absorbents, viz. aqueous ammonia (AQ_NH_3) and mono-ethanol-amine (MEA) at five different brake power values. Average carbon capture efficiency is found to be 91% and 94% with AQ_NH_3 and MEA, respectively. Further, the blend consisting of 67% of AQ_NH_3 and 33% of MEA has also been investigated which shows 95% carbon capture efficiency. This work revealed that the EGR and carbon capture unit in the Diesel engine will be an effective solution to control NO_x and CO_2 emissions simultaneously and provide the basis for future research on the execution of stringent European Standard norms.

Keywords CO_2 emission · NO_x emission · Carbon capture unit · Diesel engine

Abbreviations

AQ_NH_3	Aqueous ammonia
cc	Cubic centimeter
CCS	Carbon capture and storage
CO	Carbon monoxide
CO_2	Carbon dioxide
DMEA	Dimethyl ethanolamine
EGR	Exhaust gas recirculation
F_{dil}	Diluent effect factor
k	Kinetic energy in joule
MEA	Mono ethanolamine
NO	Nitrogen oxide
NO_2	Nitrogen dioxide
NO_x	Oxides of nitrogen
NROI	Number of particles in the sphere of influence
RNG	Renormalization group
ROI	Radius of influence in cm
SO_x	Sulphur oxide
S_L	Flame speed in m s^{-1}
U_d	Velocity (average) of the droplet in m sec^{-1}
VFD	Variable frequency drive
α	Temperature constant
β	Pressure constant
ε	Dissipation rate of turbulence in m^3 s^{-3}
Δt	Time step (s)

✉ Ajit Kumar Parwani
ajitkumar.parwani@iitram.ac.in

[1] Department of Mechanical and Aero-Space Engineering, Institute of Infrastructure Technology Research and Management, Ahmedabad 380026, India

[2] Institute of Fundamental and Frontier Sciences, University of Electronic Science and Technology of China, Chengdu 610054, Sichuan, People's Republic of China

[3] Faculty of Mechanical and Industrial Engineering, Quchan University of Technology, Quchan, Iran

Introduction

Diesel engines are widely used in locomotives, automobiles, construction, and other industrial equipment because of their high thermal efficiency and the capacity to generate high torque. In the transportation sector, the Diesel engine has a

major contribution to atmospheric pollution. The high flame temperature and surplus amount of nitrogen and oxygen during combustion lead to the formation of a significant amount of NO_x [1, 2]. Also, around 28% of global CO_2 emissions are generated from CI engines [3]. The percentage of these emissions will increase in the future, particularly in developing countries. NO_x is a highly reactive pollutant and causes photochemical smog, acid rain, and environmental degradation while CO_2 is a greenhouse gas and has the potential to cause global warming [3]. Thus, NO_x and CO_2 emissions are environmental issues and their mitigation is a challenge in the current scenario.

Research on controlling the CO_2 emissions from the Diesel engine is still under the development stage. Battery-operated vehicles, utilization of biodiesel or hydrogen in place of Diesel, temperature swing absorption technique, etc., have been projected as promising solutions [4–8]. The introduction of these technologies in the Diesel engine has helped in reducing CO_2 emissions but due to high energy penalty and loss in combustion efficiency restricted its use on a large scale [5]. Therefore, there is an urgent need to find a reliable and cheap solution, which can reduce the harmful emissions including CO_2 and NO_x without compromising the efficiency.

The thermal NO_x formation depends on the three factors, namely, the temperature inside the combustion chamber, air-fuel ratio, and the retention time of the reacting gases in the reacting zone [9–12]. The flame temperature in the range of 1500 °C to 1800 °C during the combustion process is conducive to increase the rate of reaction of nitrogen and oxygen which led to the formation of thermal NO_x. Therefore, the flame temperature should be lower than the threshold temperature of about 1100 °C [10]. Also, the time spent by the reacting gases at the maximum temperature inside the combustion chamber determines the amount of NO_x formation. If the retention time is less, then a small quantity of NO_x will be formed and vice versa [12].

Exhaust gas recirculation (EGR) is a technique where some percentage of exhaust gas is recirculated to the engine intake manifold so that the flame temperature can be reduced during combustion [13–20]. The temperature of EGR is a very important factor for the successful mitigation of NO_x. Hebbar et al. [21] performed an experimental investigation on a direct injection Diesel engine to check the effects of EGR temperature on NO_x emission and its associated effects. They found that the cooling of EGR favours the use of the higher percentage of EGR. Maiboom et al. [22] have shown that higher inlet temperature at constant EGR rate could have opposite effects on combustion and emissions, i.e., depending on operating conditions of the engine, NO_x emissions could be reduced with increased inlet temperature. Asad et al. [23] have studied the effect of EGR on the intake and in-cylinder composition of charge. Their study was based on both steady and transient operations of the engine. They found that the effectiveness of EGR to reduce NO_x is highly influenced by the EGR rate.

It can be concluded from the literature that EGR reduces NO_x emission due to thermal, chemical and dilution effects [21–24]. The thermal effect causes a reduction in combustion temperature as the specific heat of CO_2 and steam in the exhaust is high compared to nitrogen and oxygen in the fresh intake air. Oxygen from fresh air charge is diluted with inert gas, and due to this dilution effect, local flame temperature decreases. While due to the chemical effect, dissociation of recirculated CO_2 and steam takes place during combustion by an endothermic process. This dissociation reduces the flame temperature which further decreases the NO_x formation process.

The major drawback of the implementation of the EGR technique is that it increases CO_2 emissions and the amount of particulate matter [25–28]. According to Schubiger et al. [29], the premixed phase of combustion is increased due to the use of EGR which results in increased duration of combustion and ignition delay. Therefore, any unburnt CO gets converted into CO_2 due to an increase in combustion time. An EGR ratio of 40% causes extremely low emission of NO_x but it also increases the specific fuel consumption, noise level, and amount of CO_2 significantly. Hussain et al. [30] and Agrawal et al. [31] reported that a Diesel engine at low loads can tolerate high EGR because the concentration of oxygen is high in the exhaust. As the load increases, the percentage of inert gas is predominant in the exhaust, and at this condition, high EGR results in increased soot and CO_2 emissions. It was concluded that increasing the EGR ratio causes an increment in intake charge temperature while the temperature of exhaust gas reduces. There is a loss in fuel conversion efficiency, and due to the high dilution effect at high EGR, the percentage of CO_2 and CO increases. Torregrosa et al. [32] have also confirmed in their experiment on a four-stroke, four-cylinder Diesel engine that increasing the EGR ratio increases the amount of CO_2 in the exhaust.

Various CO_2 capture techniques have been developed to reduce CO_2 emissions like pre-combustion capture, oxy-fuel combustion capture, and post-combustion capture (PCC). However, these techniques were mainly focused on flue gas generated from the combustion of coal in stationary sources such as cement industries, power plants, and process industries. PCC is the most commonly used technique having an almost 90% carbon capture rate at the lowest energy penalty with suitable absorbents [33, 34] like monoethanolamine (MEA), dimethylethanolamine (DMEA), aqueous ammonia (AQ_NH_3), ionic liquids, etc. However, MEA and AQ_NH_3 are used globally because they exhibit good absorptivity at temperatures ranging from ambient temperature to 80 °C [35].

Lots of research has been done with AQ_NH_3 as an absorbent in the PCC technique. Pilot plant experiments and demonstration projects have reported the technological viability and some of the expected benefits of AQ_NH_3-based CO_2 capture processes [36–38]. The advantages include high CO_2 removal efficiency and CO_2 product purity; high stability; high CO_2 loading capacity; and high SO_2 capture effectiveness [38]. Ciferno et al. [39] performed an experimental investigation of AQ_NH_3 as an absorbent to capture CO_2 from flue gas. They found that the AQ_NH_3 has a higher loading capacity than the MEA-based process. Its low cost and formation of by-product ammonium sulphate are other benefits of the process. This process has also the potential to capture NO_x and SO_x emissions other than CO_2. Darde et al. [40] also found that ammonia as an absorbent is comparatively cheap, especially because of its energy-efficient desorption process. A recent study by Jiang et al. [41] with multi-pollutant emissions using AQ_NH_3 shows the CO_2 capture efficiency of about 84% can be achieved.

The most developed and extensively researched absorbents for carbon capture systems are amine-based absorbents. Among them, MEA is the most studied due to its high reactivity with CO_2 [39]. It is possible to capture more than 90% of CO_2 using MEA [35]. The biggest advantage of using MEA is the high reaction rate and high cyclic loading. However, the cyclic loading capacity of MEA greatly depends on temperature. An increase in temperature reduces the loading capacity of MEA [42].

From the above literature, it can be inferred that the EGR technique can significantly reduce NO_x emission but it increases CO_2 emission too. Although lots of research has been done to control NO_x emissions using the EGR method, work related to the simultaneous reduction of NO_x and CO_2 emissions is not available as per the authors' knowledge. The current research work proposes a provision to be developed in the CI engine fitted with EGR to control the NO_x emission, and carbon capture and storage (CCS) unit to capture CO_2. Literature on absorbents suggests that MEA and AQ_NH_3 are widely used absorbents for CO_2 capture in stationary coal power generation sources [35–42]. The MEA shows high capture efficiency but requires more regeneration energy [43] whereas AQ_NH_3 is economic but has moderate capture efficiency and slips easily into flue gas due to its high volatile nature [44]. Therefore, blends of AQ_NH_3 and MEA have been prepared and investigated to determine the suitable absorbent for CO_2 capture in the Diesel engine. This research work has important implications in the current scenario because European Union standard norms for reducing CO_2 emission from vehicles are becoming more stringent for the near future, i.e., it aims 15% reduction from the year 2025 and a 30% reduction from the year 2030 [45].

First, a theoretical design for an engine fitted with EGR and CO_2 capture has been presented with its general description. The current engine test rig available in the author's institute does not have a facility of EGR. Therefore, to demonstrate the effect of NO_x and CO_2 emissions with EGR, the ANSYS simulations are carried out on the combustion process of the Diesel engine with different EGR ratios. NO_x and CO_2 emissions level and temperature of the combustion chamber at different crank angles are determined with and without EGR. Finally, the experimental investigations on the exhaust of direct injection Diesel engine have been carried out for the performance evaluation of CO_2 capture at different brake power values using AQ_NH_3, MEA, and their blends.

Theoretical design and general description

The theoretical design for an engine fitted with EGR and CO_2 capture is shown in Fig. 1. The engine is slightly modified with the addition of a heat exchanger just after the exhaust manifold of the engine, and the CCS unit after the heat exchanger. Also, the fuel tank is replaced by a deadweight type accumulator.

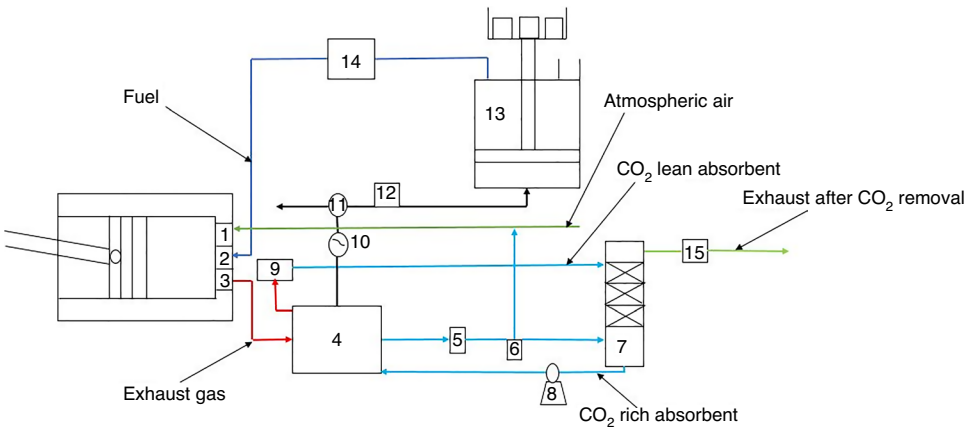

Fig. 1 Schematic of the proposed design, where the numbers represent the following parts of the design: 1-Air inlet, 2-Fuel injector, 3-Exhaust manifold, 4-Heat exchanger, 5 and 15-Temperature sensor 6-EGR valve, 7-Carbon capture unit, 8-VFD pump, 9-Air cooler, 10-Pneumatic pump, 11-Bypass valve, 12-Pressure sensor, 13-Deadweight type accumulator, and 14-Fuel injector pump

The heat exchanger placed after the exhaust manifold cools the exhaust gas to a temperature suitable for the CO_2 absorption. The sensor after the heat exchanger helps in achieving the required temperature by regulating the amount of coolant in the heat exchanger using a variable frequency drive (VFD) pump. The small percentage of exhaust gas is recirculated through the EGR valve to the intake manifold of the engine, and the remaining gas is sent to the CCS unit where CO_2 is absorbed. Captured CO_2 can be separated from the absorbent at high temperatures. Therefore, the CO_2-rich absorbent is then sent to the heat exchanger by a VFD pump where it acts as a coolant for the heat exchanger.

The heat exchanger suggested in this proposal is shell and tube type [46]. Exhaust gas is passed through the tubes and the shell is filled with coolant. The CO_2-rich absorbent gets heated when it comes into contact with exhaust gas. Absorbent releases the CO_2 in the form of a bubble after getting heat from the exhaust gas. CO_2 is then taken out from the heat exchanger using a pneumatic pump and is stored in the fuel tank which is replaced by an accumulator which is an energy storage device that stores hydraulic energy under pressure. In this proposal, a deadweight type of accumulator has been suggested to replace the fuel tank. The piston in the accumulator divides the fuel tank into two-part. Fuel is filled from the top section of the accumulator through the fuel inlet. Initially, the position of the piston remains at the bottom due to the weight of the fuel. But when the fuel is consumed due to the combustion, the piston starts moving upward, creating space in the bottom section of the accumulator. This vacant space can be utilized to store pressurized CO_2 in gas form.

While refueling at the fuel station, stored CO_2 can be taken out and filled in an outside cylinder which can be utilized for different purposes. A pressure sensor is installed before the accumulator senses the pressure inside the accumulator. If the pressure becomes high inside the accumulator, it opens the bypass valve which releases the CO_2 directly inside the atmosphere.

Combustion modeling with EGR

The simulation using the IC engine FORTE model of ANSYS 17.2 is performed for combustion in a Diesel engine to predict the exhaust emissions. The main aim of this simulation is to check the effect on NO_x and CO_2 emission with EGR. In this study, a comparison is done for a system with EGR and without EGR. The key parameters like computational domain, mesh, mathematical model, and boundary conditions required to perform simulation are detailed in the following sections.

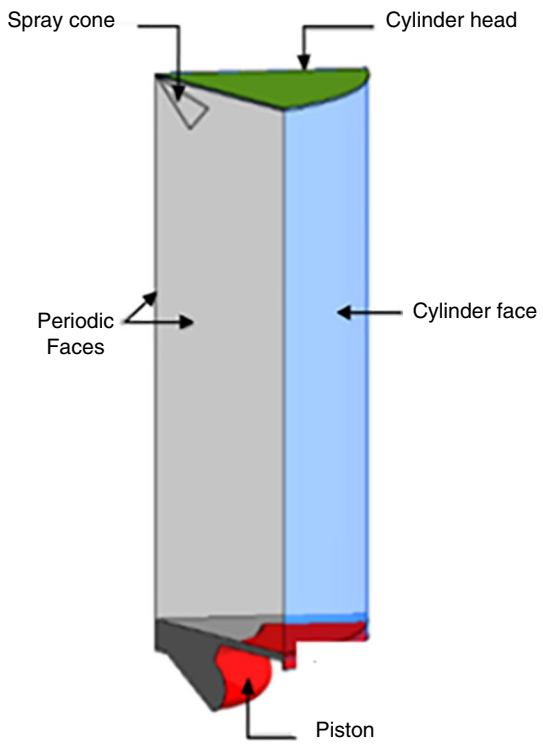

Fig. 2 Computational domain [47]

Table 1 Specifications of the computational domain

Parameters	Specifications
Spray angle	70°
Length of connecting rod	165 mm
Crank radius	55 mm
Cylinder radius	45 mm
Length of stroke	110 mm
Compression ratio	15.6
Clearance volume	4.56 mm^3 (Calculated)

Computational domain

The computational domain of the combustion chamber shown in Fig. 2 is taken from Naseer et al. [47]. The domain chosen for analysis is only 1/6th portion of the whole engine because the end faces act as periodic walls. It is assumed that the geometry of all six portions is the same, which provides the same flow rate of fuel and exerts the same pressure in all six portions [48]. It can be observed from Fig. 2 that the main constituents of the domain considered are cylinder head, cylinder wall, piston, and spray cone of fuel. The other dimensions and parameters considered for the generation of the domain are given in Table1.

Mesh generation

The computational domain is divided into different zones for generating proper mesh by using FORTE sector mesh generator. A total of 218,364 nodes and 205,320 elements are generated in the domain. The domain is discretized by using the finite volume method. Multi-zone meshing is used in which a different element size is given to each zone. A moving mesh boundary condition is given to the reciprocating piston while a periodic mesh boundary condition is given to the surfaces. The swept volume of the engine cylinder is discretized as a moving mesh or dynamic mesh, and the mesh generated near the walls is prismatic. Smoothing, layering, and re-meshing are configured for the dynamic conditions of meshing. Figure 3 shows the mesh in the computational domain at 590° crank angle.

Grid study

Table 2 shows the number of elements selected for four different grid sizes to determine the grid independence test. Figure 4 shows the results of maximum temperature attained during combustion stroke with different grid sizes for 712° to 810° crank rotation. The peak temperature value obtained at a crank angle of 730° is shown in Table 2, and the percentage error has been calculated. Grid 3 is selected for further analysis because the percentage error in peak temperature value for grid 3 and grid 4 is just 1.3%.

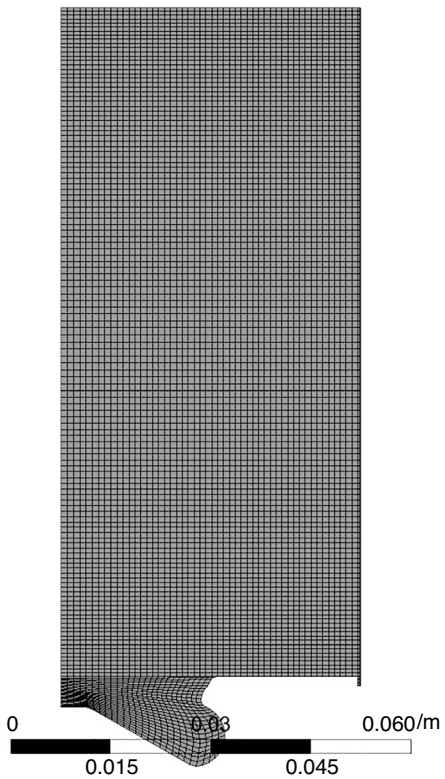

Fig. 3 Mesh in the computational domain at 590° crank angle

Table 2 Grid with different number of elements and maximum temperature value

Grid name	No of elements	Maximum temperature at 730° crank angle
Grid 1	150,850	2140
Grid 2	175,045	2210
Grid 3	205,320	2250
Grid 4	252,180	2280

Model selection

The engine considered for this modeling study is a dual-cylinder Diesel engine with 14 L of total cylinder volume. The analysis was done at an engine speed of 1500 rpm. Different mathematical models are incorporated to determine the whole combustion process. The power-law equation [49] is used to determine the flame speed (S_L^0) which can be calculated using Eq. (1)

$$S_L^0 = S_{L,ref}^0 (T/T_{ref})^{\alpha} (P/P_{ref})^{\beta} F_{dil}, \quad (1)$$

where T_{ref} and P_{ref} are the reference temperature and pressure, respectively, which are assumed to be 300 K and 1 atm. The diluent effect factor is denoted by F_{dil} and reference flame speed is denoted by $S_{L,ref}^0$ while α and β are the temperature and pressure constant, respectively. As the Diesel

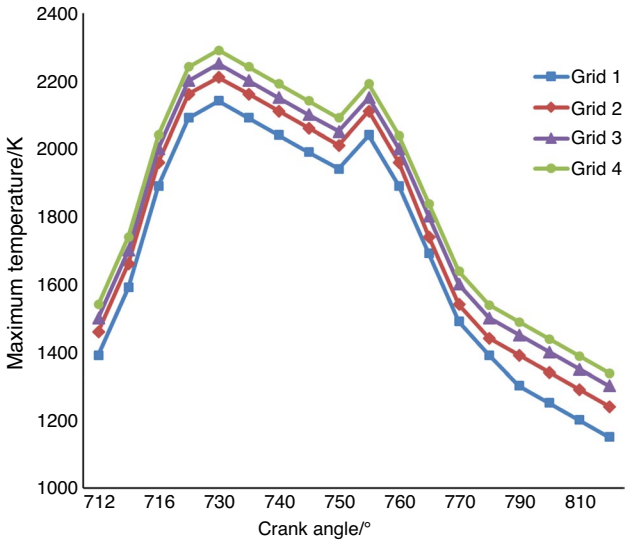

Fig. 4 Variation of maximum temperature with the crank angle at different grid sizes

engine operates on the lean mixture, Gulder [50] expression is used to determine the reference flame speed

$$S^0_{\mathrm{L,ref}} = \omega \phi^{\eta} e^{-\xi(\phi-\sigma)^2} \tag{2}$$

where ω, φ, η, ξ and σ are data-fitting coefficients. k–ε RNG model is selected for fluid turbulence in the combustion chamber. The governing equations [51] are as follows

$$\frac{\partial}{\partial t}(\rho k) + \frac{\partial}{\partial x_{\mathrm{i}}}\left(\rho k u_{\mathrm{i}}\right) = \frac{\partial}{\partial x_{\mathrm{j}}}\left(\alpha_{\mathrm{k}} \mu_{\mathrm{eff}} \frac{\partial k}{\partial x_{\mathrm{j}}}\right) + G_{\mathrm{k}} + G_{\mathrm{b}} - \rho\varepsilon - Y_{\mathrm{M}} + S_{\mathrm{k}} \tag{3}$$

$$\frac{\partial}{\partial t}(\rho \varepsilon) + \frac{\partial}{\partial}(\rho \varepsilon u_{\mathrm{i}}) = \frac{\partial}{\partial x_{\mathrm{j}}}\left(\alpha_{\varepsilon} \mu_{\mathrm{eff}} \frac{\partial \varepsilon}{\partial x_{\mathrm{j}}}\right) + C_{1\varepsilon}\frac{\varepsilon}{k}\left(G_{\mathrm{k}} + C_{3\varepsilon} G_{\mathrm{b}}\right) - C_{2\varepsilon}\rho\frac{\varepsilon^2}{k} - R_{\varepsilon} + S_{\varepsilon} \tag{4}$$

where ρ is density, k is kinetic energy, ε is the dissipation rate, U is velocity, μ_{eff} is the effective viscosity, G_{k} and G_{b} is the turbulence kinetic energy due to velocity and buoyancy respectively, Y_{M} is dilatation dissipation term, $C_{1\varepsilon}$, $C_{2\varepsilon}$, and $C_{3\varepsilon}$ are constants, α_{k} and α_{ε} are the Prandtl number for k and ε respectively, S_{k} and S_{ε} are source terms.

The radius of influence model (ROI) is used for a demonstration of Diesel spray. According to the ROI model, collision between particles is a possible only when one of the particles remains inside the radius of influence of others. The equation used to calculate the distance traveled by a spray particle within the given time step [52, 53] is given by

$$\Delta t \times U_{\mathrm{d}} = C_{\mathrm{col}} \frac{R_{\mathrm{inf}}}{N_{\mathrm{ROI}}^{1/3}} \tag{5}$$

where Δt is the time step, U_{d} is the velocity (average) of the droplet and C_{col} is the Constant, R_{inf} is the radius of influence, and N_{ROI} is the number of particles in the sphere of influence. Also, the Diesel unsteady laminar flamelet model is used for the profile of fuel injection while Diesel unsteady flamelet species model is used for the reactions during combustion.

Boundary conditions

The moving wall boundary condition is given to the piston wall since its motion depends on the movement of the crank angle (i.e., slider-crank mechanism) while the temperature of the piston is kept constant at 560 K. The temperature of the liner wall is considered as 440 K and the temperature of the wall of the cylinder head is kept as 480 K [54]. All other solid walls are considered as a no-slip boundary condition.

Initially, the pressure and temperature of the working fluid (air) are taken as 344,737.5 Pa and 404 K, respectively. The simulation starts at crank angle 570° and stops at crank angle 833°. This is the period from the inlet valve closing until the exhaust valve opening consisting only of compression and power stroke [47]. The Diesel is injected into the engine cylinder containing atmospheric air and recirculated exhaust gas. All the chemical processes were designed in a species transport model. Forty milligrams of Diesel are injected [47] and the injection of Diesel starts at 712° crank angle, which is just before the end of the compression stroke and stops at 738° crank angle.

Experimental Setup

The experimental setup (Fig. 5a) is a Mahindra 4-stroke dual cylinder, direct injection Diesel engine with a rated power of 33.57 kW at 3750 rpm. The emission from the exhaust of the engine is investigated at five different brake power. The composition of pollutants in the exhaust gas is measured by the AVL DIGAS 444 N five gas analyzer shown in Fig. 5b with the measuring range as follows.

a. CO_2—0–20% volume
b. CO—0–10% volume
c. O_2—0–22% volume
d. HC—0–20,000 ppm volume
e. NO—0–5000 ppm volume

The schematic diagram of the experimental setup is shown in Fig. 6. The variation of the load is achieved through the knob attached to the control panel connected to the eddy current dynamometer. The tailpipe of the exhaust is slightly modified to extract a secondary channel of exhaust gas. This modification is done to prevent the backpressure from the engine while performing the experiment. The exhaust from the secondary channel is directed to the carbon capture unit which consists of a gas-bubbler setup through which the exhaust gas is bubbled into the solution of absorbents. This ensures the proper mixing of exhaust gas into absorbents. The concentration of CO_2 in the exhaust is measured twice: before and after it passes through the absorbent.

Results and discussion

First, the simulation results of different parameters for the cases consisting of with and without EGR are presented. The convergence criteria of factors less than 10^{-6} are applied to each variable. This took approximately twelve hours of CPU time for each simulation. Figure 7a represents the graph of maximum temperature in the combustion chamber with the crank angle at different EGR ratios. The sudden temperature rise is observed after the 712° crank angle due to the

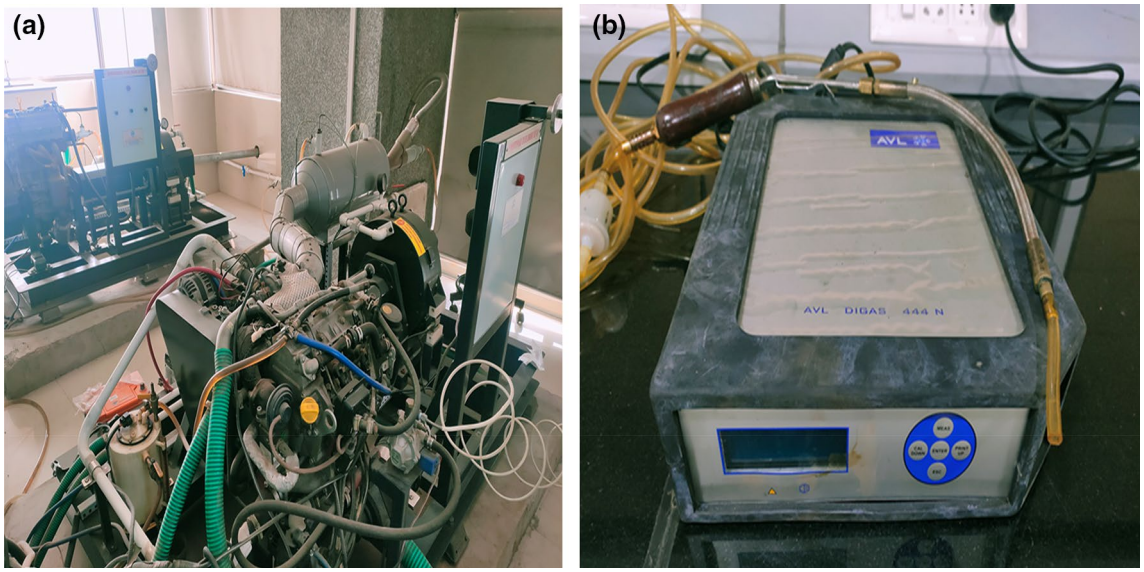

Fig. 5 Experimental setup **a** Diesel Engine **b** AVL five gas analyzer

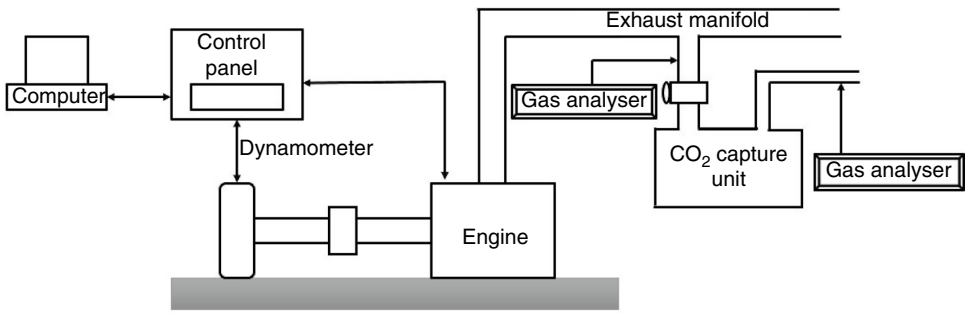

Fig. 6 Schematic of the experimental setup

initiation of combustion and formation of flame. The flame is fully developed at the peak of the curve around 730° crank angle. Figure 7a also shows that EGR significantly reduces the maximum temperature as compared to without recirculation because of the dilution of fresh air with recirculated gas at intake. The decrease of maximum temperature by 64 K, 137 K, and 199 K was observed at 10%, 20%, and 30% EGR ratio, respectively, which indicates that the drop in temperature is more with the EGR ratio of 30%. Figure 7b shows the graph of average temperature in the combustion chamber with the crank angle at different EGR ratios. This graph shows the same behavior as discussed for maximum temperature. The average temperature decrease of 2.5% is observed with 30% EGR when compared to without EGR. A similar trend of temperature decrease with EGR was also noticed by Torregrosa et al. [32], Nasser et al. [47], and Kumar et al. [55]. Figure 7a and b are magnified at the top portion of the graph to show the deviation in the curves.

Figure 8a and b represents the variation of nitrogen monoxide (NO) and nitrogen dioxide (NO_2), in the combustion chamber, respectively, with crank angles at different EGR ratios. At the start of combustion, a sharp rise in NO and NO_2 can be noticed at the 712° crank angle due to the prevalence of high temperatures. After 750° crank angle, the oxidation of NO to NO_2 takes place due to the availability of plenty of oxygen into the combustion chamber, and hence the rapid conversion of NO to NO_2 is observed. Figure 8a shows that the formation of NO decreases to 40%, 62%, and 73% as the EGR ratio increases to 10%, 20%, and 30%, respectively. This happens because when exhaust gas is recirculated, NO has also been recirculated which oxidizes to NO_2. Thus the amount of NO is reduced in the exhaust. Figure 8b shows that the formation of NO_2 reduces by 32.9%, 50.63%, and 54.43% with 10%, 20%, and 30% EGR ratios, respectively when compared to without EGR. This is because increasing the EGR ratio reduces the flame temperature which arrests the favorable environment for the formation of NO_2 reactions. A similar range of NO_x emission can be noticed in the experimental work of Zu et al. [56].

Figure 9a and b represents the variation in the amount of CO and CO_2 with the crank angle at different EGR ratios respectively. There is an average increase of 5.28%,

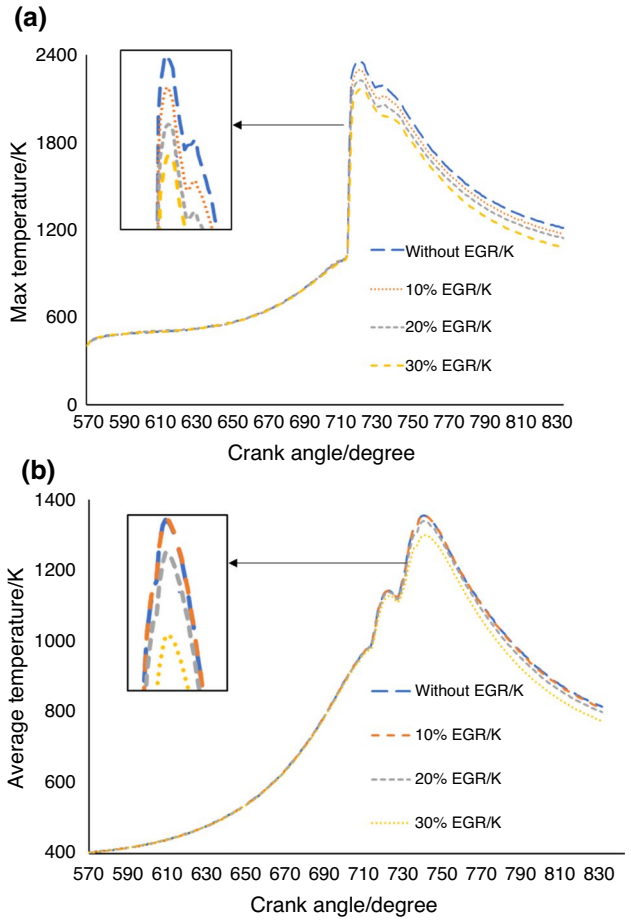

Fig. 7 Variation of **a** Maximum temperature and **b** Average temperature with crank angle at different EGR ratios

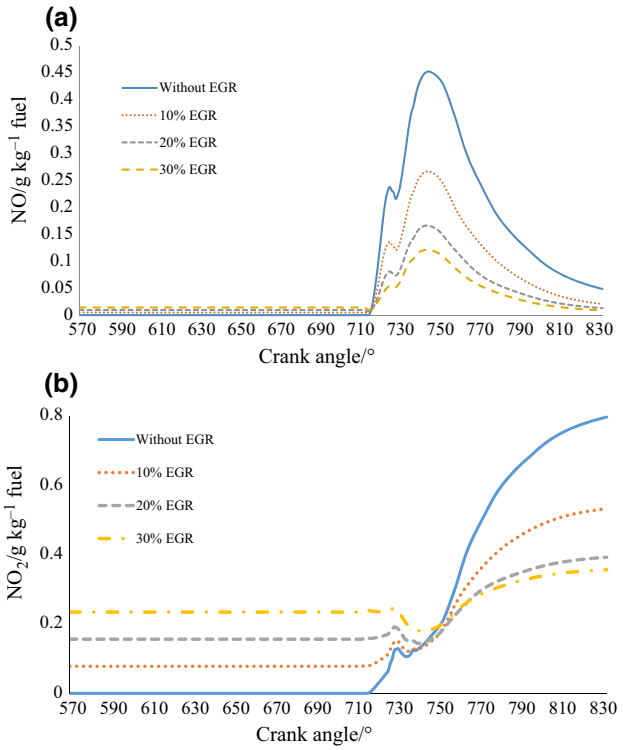

Fig. 8 Variation of **a** NO and **b** NO_2 in the combustion chamber with crank angle at different EGR ratios

42.3%, and 72.6% of CO concentration and an average increase of 4.76%, 9.52%, and 15.28% of CO_2 concentration at 10%, 20%, and 30% EGR ratio, respectively. The emission of CO is caused by incomplete combustion and is strongly influenced by the air–fuel ratio. Increased EGR rate decreases oxygen supply in the combustion chamber and slows down the reaction rates of the air–fuel mixture, resulting in lower temperatures. In such a situation, relatively lean mixtures may not be able to withstand flame propagation, resulting in higher CO emission [18, 30, 31]. The increment in CO_2 emission can be explained by the fact that fresh intake air contains negligible quantities of CO_2, while the EGR fraction contains a significant amount of CO_2, which increases with the rising EGR flow rate [21, 25]. Similar trends of the EGR effect on CO and CO_2 can be validated by the experimental work of Torregrosa et al. [32] and De Serio et al. [57].

Figure 10 shows the variation of oxygen with the crank angle at different EGR ratios. The concentration of oxygen is minimum with 30% EGR because a higher percentage of exhaust gas reduces the amount of fresh air or oxygen. With less availability of oxygen, the rate of formation of NO_x reduces.

Now the performance evaluation of carbon dioxide capture in volume percentage at different brake power with MEA, AQ_NH_3, and blends of AQ_NH_3 and MEA is presented. The CO_2 emission data from the exhaust gas without passing through any absorbent is recorded first. Then, the exhaust gas is passed through a CO_2 capture unit containing absorbents and their blends, and CO_2 emission data is recorded at the same brake power values. This process is repeated for all five brake power values. The data recorded are in percentage by volume of CO_2 emitted at different brake power with and without the capture unit. Figure 11 shows that the amount of CO_2 without capture and after capture when the exhaust gas is passed through MEA, AQ_NH_3, and a blend of 67% AQ_NH_3 and 33% MEA by volume. The blend composition has been selected such that its capture efficiency is similar to standalone MEA absorbent and hence reduces the cost of absorbent. It can be observed that the amount of CO_2 after passing through the blend of AQ_NH_3 and MEA is minimum as compared to standalone absorbents MEA and AQ_NH_3. This shows that the blend of AQ_NH_3 and MEA has absorbed maximum CO_2 compared to MEA and AQ_NH_3. On average, the capture efficiency of MEA, AQ_NH_3 and their blend is 94%, 91% and 95%, respectively.

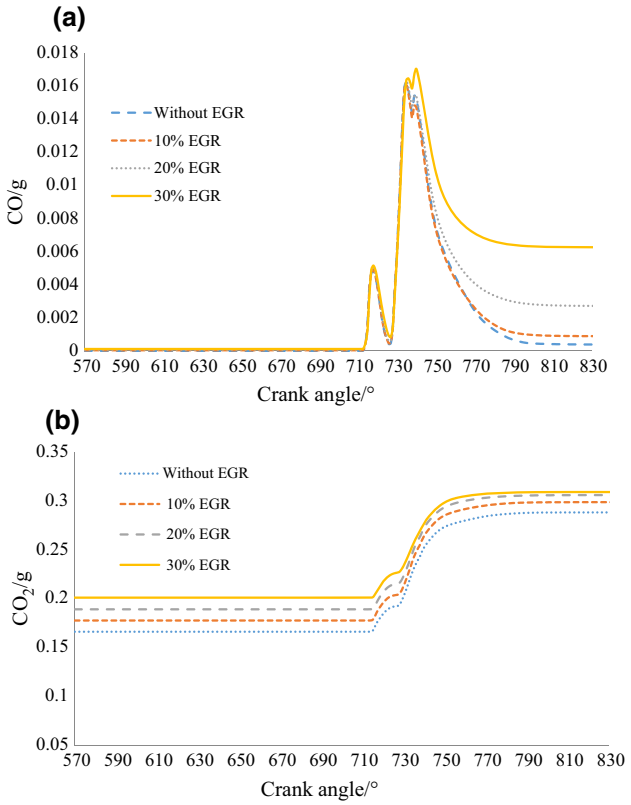

Fig. 9 Variation of **a** CO and **b** CO_2 with crank angle at different EGR ratios

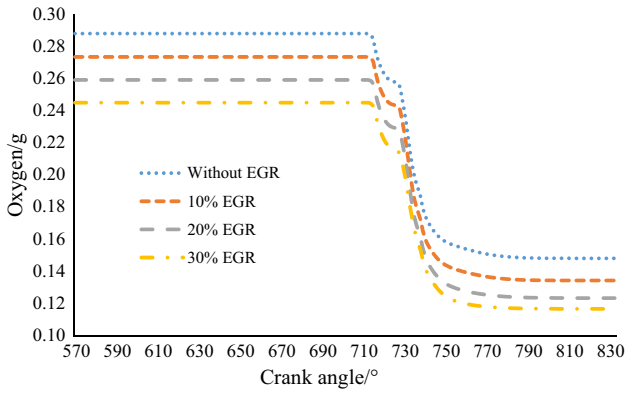

Fig. 10 Variation of oxygen with crank angle at different EGR ratios

The capture efficiency refers to the ratio of the amount of CO_2 absorbed by the absorbent to the amount of CO_2 present before the absorbent. Also, the trend of the graph shows that as the brake power increases, the amount of CO_2 after passing through absorbent increases significantly. This is because, at higher brake power, CO_2 emission increases, and the absorbent reaches its saturation value at ambient pressure and temperature condition. This problem can be avoided by continuously

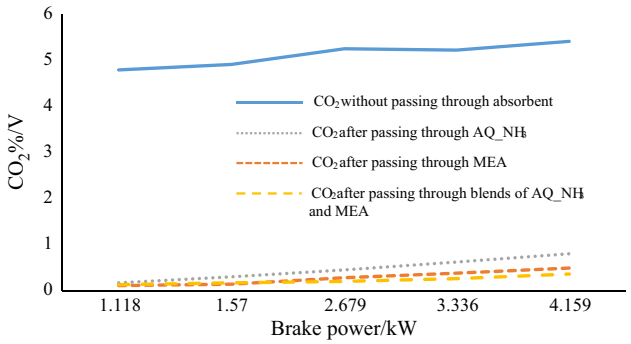

Fig. 11 Percentage by volume of CO_2 in the exhaust gas without and after capture by absorbents

Table 3 Accuracy and uncertainty of the experiment

Measuring instrument	Accuracy
Dynamometer	Torque: ± 0.5 Nm Speed: ± 2 rpm
Fuel flow meter	± 0.12%
Air flow meter	± 1%
Gas analyzer (CO_2 measurement)	± 0.5% Measuring range: 0–20% volume
Thermocouple (K type)	± 1 °C
Computed parameters	Uncertainty
Brake power	± 1.46%
BSFC	± 1.01%
Thermal efficiency	± 1.21%

circulating the fresh absorbent from the regeneration of saturated solvent in the stripper column of the capture unit.

Experimental conditions, observations, instrument calibration, test assembly, etc. are the major parameters that affect the results of any experiment. Therefore, uncertainty analysis is very important to validate the accuracy of the experiment. Reliability of any measuring device which also refers to instrument accuracy is provided by the instrument manufacturers. Table 3 summarizes the accuracy and uncertainty of the experiment while Table 4 shows the uncertainty level in the calculation of brake power by the linearized approximation method of uncertainty [58].

Conclusions

The focus of this research work is to explore a reliable solution to cope with rising global warming and atmospheric pollution. The severity of this problem can also be attributed to the fact that European Union norms for CO_2 reduction from vehicles will become more stringent in the coming years. With this motivation, a theoretical design has been

Table 4 Uncertainty level calculation for BP

RPM	Brake power			Max. and Min. value		Accuracy ± 0.06		Average	% Uncertainty	
	Test1/kW	Test2/kW	Test3/kW	Max./kW	Min./kW	Max. + 0.06	Min. − 0.06		+	−
	A	*B*	*C*	*D*	*E*	$F=D+0.06$	$G=E-0.06$	$H=(F+G)/2$	$I=\{(F-H)/H\}*100$	$J=\{(H-G)/H\}*100$
1000	4.00	4.01	4.03	4.03	4.00	4.09	3.94	4.015	1.86	− 1.86
1300	5.28	5.29	5.30	5.30	5.28	5.36	5.22	5.29	1.32	− 1.32
1600	6.09	6.16	6.20	6.20	6.09	6.26	6.03	6.145	1.87	− 1.87
1900	6.91	6.88	6.93	6.93	6.88	6.99	6.82	6.905	1.23	− 1.23
2200	7.55	7.61	7.65	7.65	7.55	7.71	7.49	7.6	1.44	− 1.44
2500	8.64	8.69	8.62	8.69	8.62	8.75	8.56	8.655	1.09	− 1.09
Uncertainty level of BP									+ 1.46%	− 1.46%

proposed to reduce NO_x emissions and capture CO_2 with little modifications to the engine. An EGR method for control of NO_x has been studied numerically and analysis of temperature and emissions is presented at different crank angles and EGR ratios. The numerical analysis shows that although EGR reduces the NO_x emission successfully, it increases the CO_2 emission. Therefore, to address this problem, the post-combustion carbon capture method has been experimentally investigated to capture the CO_2 from the exhaust of the Mahindra direct injection Diesel engine. The major outcomes of the work are listed below:

1. The in-cylinder maximum temperature decreases by 64 K, 137 K, and 199 K at 10%, 20%, and 30% EGR ratio, respectively. Similar trends are observed with average temperature. Temperature reduction causes an average of 50% reduction in NO_x emission.
2. The average CO concentration increase of 5.28% at 10% EGR, 42.3% at 20% EGR, and 72.6% at 30% EGR is observed. While an increment of 4.76%, 9.52%, and 15.28% in CO_2 concentration at 10%, 20%, and 30% EGR ratio, respectively, is observed.
3. The amount of oxygen concentration in the exhaust gas is minimum at 30% EGR. This is also one of the reasons behind the decrease in the rate of formation of NO_x.
4. MEA, AQ_NH_3, and blend of 67% AQ_NH_3 and 33% MEA shows average capture efficiency of 94%, 91%, and 95%, respectively. Therefore, the blend shows maximum absorption efficiency at a minimum cost.

The experiment with EGR has been left for further study. However, the results of this study are satisfactory and motivate the practitioners to conduct experiments on the proposed theoretical design of the engine for simultaneous reduction of NO_x and CO_2. The effect of CO_2 capture with different EGR ratios could also be a part of future studies.

Author contributions All authors contributed to the study conception and design. Material preparation and data collection were performed by PK. Analysis was done by PK, AKP, MMR. The first draft of the manuscript was written by PK, and all authors commented on previous versions of the manuscript. All authors read and approved the final manuscript.

References

1. Zelenka P, Aufinger H, Reczek W, Cartellieri W. Cooled EGR—a key technology for future efficient HD diesels. In: SAE Technical Papers. SAE International; 1998.
2. Hoard J, Abarham M, Styles D, Giuliano JM, Sluder CS, Storey John ME. Diesel EGR cooler fouling. SAE Int J Engines. 2008;1(1):1234–50.

3. Jang S, Park S, Choi K, Kim H. Experimental investigation of the influences of shape and surface area on the EGR cooler efficiency. Heat Mass Transf. 2011;47(6):621–8.
4. Hoseinzadeh S, Stephan HP. Advanced energy, exergy, and environmental (3e) analyses and optimization of a coal-fired 400 mw thermal power plant. J Energy Resour Technol. 2021;143(8):082106.
5. Sharma S, Maréchal F. Carbon dioxide capture from internal combustion engine exhaust using temperature swing adsorption. Front Energy Res. 2019;7:143.
6. Avsec J, Wang ZL, Naterer GF. Thermodynamic and transport properties of fluids and solids in a Cu-Cl solar hydrogen cycle. J Therm Anal Calorim. 2017;127:961–7.
7. Xie HQ, Yu QB, Zuo ZL, Zhang JR, Han ZC, Qin Q. Thermodynamic analysis of hydrogen production from raw coke oven gas via steam reforming. J Therm Anal Calorim. 2016;3:1621–31.
8. Zhang HY, Xiao R, Song M, Shen DK, Liu J. Hydrogen production form bio-oil by chemical looping reforming. J Therm Anal Calorim. 2014;115:1921–7.
9. Turns SR. An introduction to combustion. New York: McGraw-Hill; 1996. p. 286.
10. Hountalas DT, Mavropoulos GC, Binder KB. Effect of exhaust gas recirculation (EGR) temperature for various EGR rates on heavy duty DI diesel engine performance and emissions. Energy. 2008;33:272–83.
11. Dangar H, Rathod GP. Combine effect of exhaust gas recirculation (egr) and varying inlet air pressure on performance and emission of diesel engine. IOSR J Mech Civ Eng (IOSR-JMCE). 2013;6(5):26–33.
12. Semakula M, Inambao F. The formation, effects and control of oxides of nitrogen in diesel engines. Int J Appl Eng Res. 2018;13(6):3200–9.
13. Park SH, Junepyo C, Lee CS. Effects of bioethanol blended diesel fuel on combustion and emission reduction characteristics in a direct-injection diesel engine with exhaust gas recirculation (EGR). Energy Fuel. 2010;24(7):3872–83.
14. Park SH, Youn IM, Lee CS. Influence of two-stage injection and exhaust gas recirculation on the emissions reduction in an ethanol-blended diesel-fueled four-cylinder diesel engine. Fuel Process Technol. 2010;91:1753–60.
15. Ishida M, Yamamoto S, Ueki H, Sakaguchi D. Remarkable improvement of NO_x-PM trade-off in a diesel engine by means of bioethanol and EGR. Energy. 2010;35:4572–81.
16. He BQ. Advances in emission characteristics of diesel engines using different biodiesel fuels. Renew Sustain Energy Rev. 2016;60:570–86.
17. Divekar PD, Chen X, Tjong J, Zheng M. Energy efficiency impact of EGR on organizing clean combustion in diesel engines. Energy Convers Manag. 2016;112:369–81.
18. Kumar BR, Saravanan S, Rana D, Anish V, Nagendran A. Effect of a sustainable biofuel—n-octanol—on the combustion, performance and emissions of a DI diesel engine under naturally aspirated and exhaust recirculation (EGR) modes. Energy Convers Manag. 2016;118:275–86.
19. Bozza F, De Bellis V, Teodosio L. Potentials of cooled EGR and water injection for knock resistance and fuel consumption improvements of gasoline engines. Appl Energy. 2016;169:112–25.
20. Mohammadi A, Ishiyama T, Kakuta T, Kee SS. Fuel injection strategy for clean diesel engine using ethanol blended diesel fuel. SAE Technical Papers Series. 2005;01-1725.
21. Hebbar GS, Bhat AK. Control of NO_x from a DI diesel engine with hot EGR and ethanol fumigation: an experimental investigation. Int J Automot Technol. 2013;14:333–41.
22. Maiboom A, Tauzia X, Hétet JF. Experimental study of various effects of exhaust gas recirculation (EGR) on combustion and emissions of an automotive direct injection diesel engine. Energy. 2008;33:22–34.
23. Asad U, Zheng M. Exhaust gas recirculation for advanced diesel combustion cycles. Appl Energy. 2014;123:242–52.
24. Millo F, Giacominetto PF, Bernardi MG. Analysis of different exhaust gas recirculation architectures for passenger car diesel engines. Appl Energy. 2012;98:79–91.
25. Zheng M, Reader GT, Hawley JG. Diesel engine exhaust gas recirculation—a review on advanced and novel concepts. Energ Convers Manag. 2004;45:883–900.
26. Li X, Xu Z, Guan C, Huang Z. Impact of exhaust gas recirculation (EGR) on soot reactivity from a diesel engine operating at high load. Appl Therm Eng. 2014;68:100–6.
27. Fang Q, Fang J, Zhuang J, Huang Z. Influences of pilot injection and exhaust gas recirculation (EGR) on combustion and emissions in a HCCI-DI combustion engine. Appl Therm Eng. 2012;48:97–104.
28. Hoseini SS, Najafi G, Ghobadian B, Yusaf T, Mamat R. Experimental and numerical analysis of flow and heat transfer characteristics of EGR cooler in diesel engine. Appl Therm Eng. 2018;140:745–58.
29. Schubiger R, Bertola A, Boulouchos K. Influence of EGR on combustion and exhaust emissions of heavy duty DI-diesel engines equipped with common-rail injection systems. SAE Techn Pap Ser. 2001; 01-3497.
30. Hussain J, Palaniradja K, Alagumurthi N, Manimaran R. Effect of exhaust gas recirculation (EGR) on performance and emission characteristics of a three-cylinder direct injection compression ignition engine. Alex Eng J. 2012;51:241–7.
31. Agarwal D, Singh SK, Agarwal AK. Effect of exhaust gas recirculation (EGR) on performance, emissions, deposits and durability of constant speed compression ignition engine. Appl Energy. 2011;8:2900–7.
32. Torregrosa AJ, Broatch A, Olmeda P, Salvador-Iborra J, Warey A. Experimental study of the influence of exhaust gas recirculation on heat transfer in the firedeck of a direct injection diesel engine. Energy Convers Manag. 2017;153:304–12.
33. Cormos CC. Assessment of chemical absorption/adsorption for post-combustion CO_2 capture from Natural Gas Combined Cycle (NGCC) power plants. Appl Therm Eng. 2015;82:120–8.
34. Koronaki IP, Prentza L, Papaefthimiou VD. Parametric analysis using AMP and MEA as aqueous solvents for CO_2 absorption. Appl Therm Eng. 2017;110:126–35.
35. Kumar P, Rathod V, Parwani AK. Experimental investigation on performance of absorbents for carbon dioxide capture from diesel engine exhaust. Environ Prog Sustain Energy. 2021;40:13651.
36. Jonsson S, Telikapalli V. Chilled Ammonia Process installed at the Technology Center Mongstad. 11st International Conference on Greenhouse Gas Control Technologies (GHGT-11), Kyoto, Japan, 18–22 Nov 2012.
37. Rhee CH, Kim JY, Han K, Ahn CK, Chun HD. Process analysis for ammonia-based CO_2 capture in ironmaking industry. Energy Procedia. 2011;4:1486–93.
38. Yu H, Morgan S, Allport A, Cottrell A, Do T, McGregor J, Feron P. Results from trialling aqueous ammonia based post combustion capture in a pilot plant at Munmorah. Energy Procedia. 2011;4:1294–302.
39. Ciferno JP, DiPietro P,Tarka T. An economic scoping study for CO_2 capture using aqueous ammonia. National Energy Technology Laboratory, 2005.
40. Darde V, Thomsen K, van Well WJM, Stenby EH. Chilled ammonia process for CO_2 capture. Energy Procedia. 2009;1(1):1035–42.
41. Jiang K, Yu H, Chen L, Fang M, Azzi M, Cottrell A, Li K. An advanced, ammonia-based combined $NO_x/SO_x/CO_2$ emission

control process towards a low-cost, clean coal technology. Appl Energy. 2020;260:114316.
42. Galindo P, Schäffer A, Brechtel K, Unterberger S, Scheffknecht G. Experimental research on the performance of CO_2-loaded solutions of MEA and DEA at regeneration conditions. Fuel. 2012;101:2–8.
43. Liang Z, Rongwong W, Liu H, Fu K, Gao H, Cao F, et al. Recent progress and new developments in post-combustion carbon-capture technology with amine based solvents. Int J Greenhouse Gas Control. 2014;50:26–54.
44. Budzianowski W, Koziol A. Stripping of ammonia from aqueous solutions in the presence of carbon dioxide: effect of negative enhancement of mass transfer. Chem Eng Res Des. 2005;83:196–204.
45. European Commission. Setting CO_2 emission performance standards for new heavy-duty vehicles and amending Regulations (EC) No 595/2009 and (EU) 2018/956 of the European Parliament and of the Council and Council Directive 96/53/EC. 2019 https://eur-lex.europa.eu/eli/reg/2019/1242/oj. Accessed 8 February 2021.
46. Hoseinzadeh S, Heyns PS. Thermo-structural fatigue and lifetime analysis of a heat exchanger as a feedwater heater in power plant. Eng Fail Anal. 2020;113:104548.
47. Naseer A, Hanumanth Rao AV, Atgur V, Moulali S, Manavendra G. Numerical studies on combustion characterization of four stroke diesel engine. Int J Veh Struct Syst. 2019;9(6):234–40.
48. Abay K, Colak U, Yüksek L. computational fluid dynamics analysis of flow and combustion of diesel engine. J Therm Eng. 2018;4(2):1878–95.
49. Metghalchi M, Keck JC. Burning velocities of mixtures of air with methanol, isooctane, and indolene at high pressure and temperature. Combust Flame. 1983;48:191–210.
50. Gülder Ö. Correlations of laminar combustion data for alternative s.i. engine fuels. SAE Technical Paper. 1984;841000.
51. Yakhot V, Orszag SA, Thangam S, Gatski TB, Speziale CG. Development of turbulence models for shear flows by a double expansion technique. NASA Contractor Report 187611 S E.,ICASE.1992;4(7):91–65.
52. Munnannur A, Reitz RD. A comprehensive collision model for multi-dimensional engine spray computations. Atomiz Sprays. 2009;19:597–619.
53. Munnannur A, Reitz RD. Droplet collision modeling in multi-dimensional engine spray computations. International multidimensional engine modeling user's group meeting at the sae congress. 2007.
54. Makadia U, Kumar P, Parwani AK, Deb D. Simulations of exhaust gas recirculation and its impact on NOx. In: Deb D, Balas V, Dey R, editors. Innovations in Infrastructure. Adv in Intel Sys and Comp. 2019; p. 757.
55. Kumar JTS, Sharma TK, Murthy KM, Rao GAP. Effect of reformed EGR on the performance and emissions of a diesel engine: a numerical study. Alex Eng J. 2018;57(2):517–25.
56. Zu XH, Yang CL, Wang HC, Wang YY. Experimental study on diesel engine exhaust gas recirculation performance and optimum exhaust gas recirculation rate determination method. R Soc Open Sci. 2019;6(6):181907.
57. De Serio D, de Oliveira A, Sodré JR. Effects of EGR rate on performance and emissions of a diesel power generator fueled by B7. J Braz Soc Mech Sci Eng. 2017;39(6):1919–27.
58. Ruhul AM, Kalam MA, Masjuki HH, Alabdulkarem A, Atabani AE, Fattah IMR, Abedin MJ. Production, characterization, engine performance and emission characteristics of Croton megalocarpus and Ceiba pentandra complementary blends in a single-cylinder diesel engine. RSC Adv. 2016;6(29):24584–95.